Fourier analysis of the nuclear flux density in diatomic molecules: A complementary tool to map potential-energy curves and to characterize vibrational wave functions

Jhon Fredy Pérez-Torres*

Institut für Chemie und Biochemie, Freie Universität Berlin, Takustraße 3, 14195 Berlin, Germany

(Received 3 December 2014; published 17 February 2015)

Pump-probe spectroscopy has allowed the construction of the nuclear probability density $\rho(R,t)$ as a function of the internuclear bond distance (R) and the time (t) in diatomic molecules and consequent deduction of the nuclear flux density $j(R,t)$. Thus, the two observables $[\rho(R,t), j(R,t)]$ comprise a very detailed description of the nuclear motion in ultrafast molecular dynamics. Here a Fourier analysis of $j(R,t)$ is proposed and compared with the already existing Fourier analysis of $\rho(R,t)$. It is shown that the two power spectra $|\tilde{\rho}(R,\omega;T)|^2$ and $|\tilde{j}(R,\omega;T)|^2$ provide the same information in the frequency domain ω, but entirely different information in the spatial domain (i.e., along the R coordinate).

DOI: 10.1103/PhysRevA.91.022510 PACS number(s): 33.20.Tp, 32.80.Rm, 33.80.Rv, 82.53.−k

I. INTRODUCTION

Pump-probe spectroscopy, the most common technique in femtosecond chemistry, has allowed the construction of $\rho(R,t)$ in diatomic molecules, for instance, in the Na_2 molecule vibrating in the excited state $2^1\Pi_g$ [1], and in the D_2^+ molecular ion vibrating in the ground state $^2\Sigma_g^+$ [2]. In a pump-probe experiment, a pump pulse is used to excite or ionize a molecule. Consequently a nuclear wave packet is immediately launched and propagated in an excited state of the molecule or in the ground state of the molecular ion. Then a delayed probe pulse monitors the wave packet, e.g., by dissociation of the vibrating molecule. Experimentally, the kinetic energy of the charged fragments is recorded [kinetic energy release (KER) spectrum] as a function of the time delay between the pump and probe pulses. The nuclear probability density $\rho(R,t)$ is then constructed from the KER spectrum by using the Coulomb law, as established in Ref. [4]. This technique has provided detailed information about molecular vibrations, for instance observation of the dephasing and the revival [5,6] of the nuclear wave packet [2,7].

During the field-free propagation of the wave packet the time-dependent nuclear wave function can be represented as a coherent superposition of vibrational eigenstates $\chi_n(R)$ of the nuclear Hamiltonian,

$$\Psi(R,t) = \sum_n c_n \chi_n(R) e^{-iE_n t/\hbar}. \tag{1}$$

The set of constant coefficients $\{c_n\}$ is determined by the initial wave packet $\Psi(R,0)$. The two R-dependent observables of concern here are the nuclear probability density

$$\rho(R,t) = \sum_{mn} c_m c_n \cos(\omega_{mn} t)\chi_m(R)\chi_n(R) \tag{2}$$

and the nuclear flux density

$$j(R,t) = \frac{\hbar}{\mu_n} \sum_{mn} c_m c_n \sin(\omega_{mn} t)\chi_m(R)\frac{d}{dR}\chi_n(R), \tag{3}$$

where μ_n is the reduced mass of the nuclei and $\omega_{mn} = (E_m - E_n)/\hbar$ is the Bohr frequency. Alternatively, the nuclear flux density $j(R,t)$ can be obtained from the nuclear probability density $\rho(R,t)$ by means of the continuity equation [8]. In fact, the continuity equation was recently used to deduce an experimental nuclear flux density [3], which revealed several novel quantum effects for the first time. Thus, the two observables, the probability density and the flux density, comprise a very detailed (space- and time-resolved) description of vibrations in molecular dynamics.

It is instructive to supplement the description of the molecular vibration on the space-time domain provided by $\rho(R,t)$ and $j(R,t)$ with its space-frequency counterpart. Thus, by Fourier transforming the nuclear probability density and the nuclear flux density separately for each internuclear distance R, the Fourier power spectra (also referred to as quantum beat spectra) are obtained. Here we illustrate these ideas first by quantum-dynamical calculations in the $D_2^+(^2\Sigma_g^+)$ molecular ion, and then we apply the concepts to the available experimental fluxes (the D_2^+ and Na_2 molecules) reported in the literature [3].

II. THEORY

The Fourier transform of $\rho(R,t)$ and $j(R,t)$ read:

$$\begin{aligned}\tilde{\rho}(R,\omega;T) &= \frac{1}{\sqrt{2\pi}}\int_0^T \rho(R,t)e^{-i\omega t}dt \\ &= \frac{1}{\sqrt{2\pi}}\sum_{mn} c_m c_n \chi_m(R)\chi_n(R) \\ &\quad\times \int_0^T \cos(\omega_{mn}t)e^{-i\omega t}dt\end{aligned} \tag{4}$$

and

$$\begin{aligned}\tilde{j}(R,\omega;T) &= \frac{1}{\sqrt{2\pi}}\int_0^T j(R,t)e^{-i\omega t}dt \\ &= \frac{1}{\sqrt{2\pi}}\sum_{mn} c_m c_n \chi_m(R)\frac{d}{R}\chi_n(R) \\ &\quad\times \int_0^T \sin(\omega_{mn}t)e^{-i\omega t}dt,\end{aligned} \tag{5}$$

respectively. The Fourier transform of the probability density Eq. (4) was used to analyze $\rho(R,t)$ constructed from

*jperez@zedat.fu-berlin.de

experimental data for the vibrating D_2^+ molecular ion [9]. It has also been applied to quantum-dynamical calculations on a wide set of prototypal diatomic molecules [10]. For each internuclear distance the power spectra display different groups of frequencies. At low frequencies the group with $\omega_{m,n=m+1}$ appears, followed by the second group with $\omega_{m,n=m+2}$ and so on. If T is long enough, each individual value of ω_{mn} in the group can be resolved to reveal the product of two vibrational eigenstates $c_m c_n \chi_m(R)\chi_n(R)$ when the R dependence of the power spectrum is analyzed. For $T \to \infty$, $\int_0^T \cos(\omega_{mn}t)e^{-i\omega t}dt$ and $\int_0^T \sin(\omega_{mn}t)e^{-i\omega t}dt$ are described in terms of the Dirac δ function, yielding power spectra with infinitely fine resolution. From such an analysis, one can map the intramolecular potential energy, or more precisely, the derivative of potential energy curve in which the wave packet is being propagated [9–11].

III. RESULTS

In order to illustrate our theory, we consider the propagation of a nuclear wave packet in the $^2\Sigma_g{}^+$ electronic ground state of a D_2^+ molecular ion, initiated, for example, by the photoionization of a D_2 molecule. Figure 1(a) displays the power spectrum for the calculated probability density of the D_2^+ molecular ion vibrating in the $^2\Sigma_g{}^+$ electronic state. The coefficients $\{c_n\}$ correspond to the Franck-Condon factors between the vibrational eigenfunction $\Phi(R)$ of the electronic ground state of the D_2 and the vibrational eigenfunctions of the D_2^+, i.e., $c_n = \langle \chi_n | \Phi \rangle$. Details of the calculation of the potential energy curves and the eigenfunctions can be found in Ref. [12]. Detailed interpretation of the power spectrum of the probability density for this system is given in Refs. [9–11]. However, for the sake of a self-contained presentation, we summarize the main features of this power spectrum here. The left panel of Fig. 1(a) exhibits a series $|\chi_m(R)\chi_{n=m+1}(R)|^2$ corresponding to the quantum beats between successive vibrational eigenstates. For example, at $\omega_{0,1} = 47.3$ THz the quantum beat $|\chi_0(R)\chi_1(R)|^2$ appears, exposing the node of the $\chi_1(R)$ vibrational eigenstate around $R \sim 2a_0$. At $\omega_{1,2} = 45.4$ THz the quantum beat $|\chi_1(R)\chi_2(R)|^2$ appears with three nodes, one from the $\chi_1(R)$ eigenstate and two from the $\chi_2(R)$ eigenstate, and so on. Hence, each frequency displays a nodal structure along the internuclear distance, and the boundaries of $|\chi_n(R)\chi_m(R)|^2$ depict the potential energy curve as can be seen from Fig. 1(a).

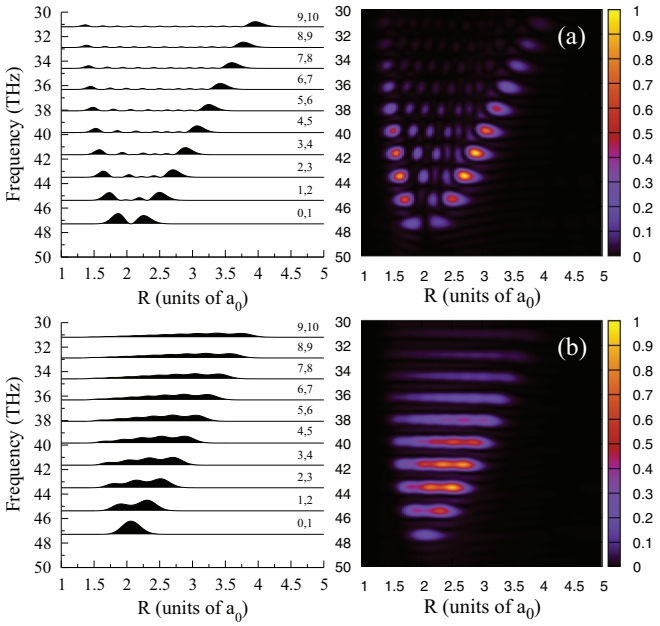

FIG. 1. (Color online) Power spectra of a D_2^+ molecular ion vibrating in the $^2\Sigma_g{}^+$ electronic state: (a) power spectrum of the calculated nuclear probability density $[|\tilde{\rho}(R,\omega;T = 1200\,\text{fs})|^2]$, (b) power spectrum of the calculated nuclear flux density $[|\tilde{j}(R,\omega;T = 1200\,\text{fs})|^2]$. On the left $|\chi_m(R)\chi_n(R)|^2$ (upper panel) and $|\chi_m(R)d\chi_n(R)/dR - \chi_n(R)d\chi_m(R)/dR|^2$ (lower panel).

We turn our attention now to the power spectrum of the flux density [see Fig. 1(b)]. As in the case of the probability density, the Bohr frequencies are revealed. However, the R dependence is quite different [compare Eq. (4) with Eq. (5)]. Now what is observed along the internuclear distance is proportional to $|\chi_m(R)d\chi_n(R)/dR - \chi_n(R)d\chi_m(R)/dR|^2$ instead of $|\chi_m(R)\chi_n(R)|^2$. It is noteworthy that the new R dependence of the power spectrum displays no nodes for any couple (m,n) of eigenstates, as can be seen from the left panel of Fig. 1(b). Notice that the power spectrum of the flux density supplements the spectrum of the probability density, in the sense that the power spectrum of the probability density exposes the inner and outer turning points of the potential, while the power spectrum of the flux density exposes a structure between the turning points with several maxima and minima corresponding to the inflection points (where the first derivative takes extreme values) of the eigenstates. For example, the quantum beat at $\omega_{0,1} = 47.3$ THz displays a maximum around $R \sim 2a_0$. At this internuclear distance, the maximum value of $\chi_0(R)$ and one of the inflection points of $\chi_1(R)$ match [see Fig. 2(a)]. The inflection points of $\chi_0(R)$ almost match with the maximum and minimum values of $\chi_1(R)$ [see Fig. 2(b)], although they are overlapped by the dominant distribution $|\chi_0(R)d\chi_1(R)/dR|^2$, thus rendering this contribution imperceptible [see above Fig. 2(a), where $|\chi_0(R)d\chi_1(R)/dR - \chi_1(R)d\chi_0(R)/dR|^2$ is displayed]. At the second quantum beat ($\omega_{1,2} = 45.4$ THz), two of the inflection points of $\chi_2(R)$ are magnified by the maximum and minimum values of $\chi_1(R)$ [see Fig. 2(c)], while the inflection points of $\chi_1(R)$, magnified by the maximum and minimum values of $\chi_2(R)$ [see Fig. 2(d)], become imperceptible [see above Fig. 2(c), where $|\chi_1(R)d\chi_2(R)/dR - \chi_2(R)d\chi_1(R)/dR|^2$ is displayed]. In summary, the first quantum beat exposes the inflection point of the eigenstate $\chi_1(R)$ together with the maximum value of $\chi_0(R)$, the second quantum beat exposes two of the inflection points of the eigenstate $\chi_2(R)$ together with the maximum values of $\chi_1(R)$, and so on.

To demonstrate the practicability of the formalism, we need to construct $j(R,t)$ from experimental data. For instance, the flux density $j(R,t)$ can be obtained from the density $\rho(R,t)$ by means of the continuity equation [8] together with the proper boundary conditions, according to $j(R,t) = -\partial_t \int_0^R dR' \rho(R',t)$. A more detailed description can be found in the original paper by Manz and coworkers [3]. There, the flux density is deduced from original measurements of $\rho(R,t)$ by Frohnmeyer and Baumert for $Na_2(^2\Pi_g)$ [1] as

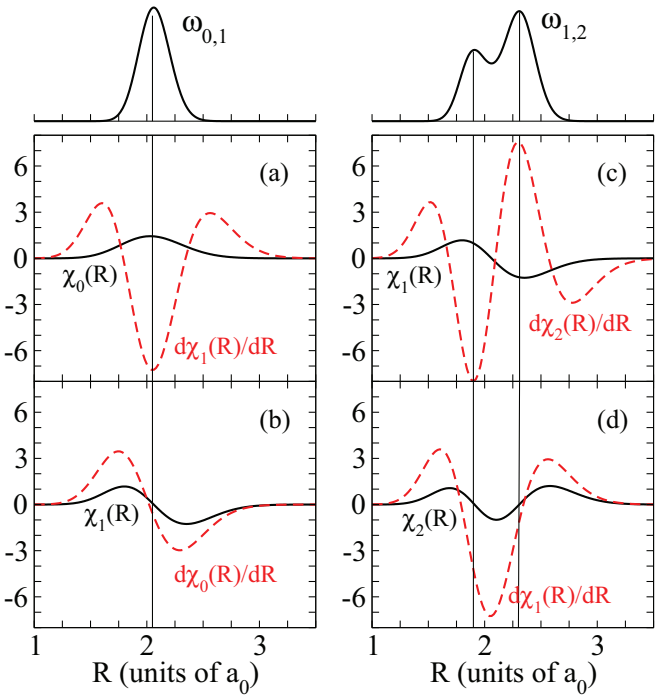

FIG. 2. (Color online) Wave functions $\chi_0(R)$, $\chi_1(R)$ and $\chi_2(R)$ and their corresponding derivatives $d\chi_0(R)/dR$, $d\chi_1(R)/dR$ and $d\chi_2(R)/dR$. On top, the components $\omega_{0,1}$ and $\omega_{1,2}$ of the power spectrum of the flux density $[|\tilde{j}(R,\omega;T=1200\,\text{fs})|^2]$ are shown. The vertical lines indicate the position of the maxima of the power spectrum.

well as by Ullrich, Moshammer, and coworkers for D_2^+ [2]. Figures 3(a) and 3(b) display, respectively, the power spectra for the constructed nuclear probability density [2] and the deduced nuclear flux density [3] of the D_2^+ molecular ion. The power spectrum of the probability density differs from the previous calculations (see Fig. 1) mainly because of the field dressing of the molecular ion by the extremely intense ($I_{\max} \sim 0.5 \times 10^{15}\text{W/cm}^2$) laser pulse [2,13]. Since the power spectrum of the probability density $|\tilde{\rho}(R,\omega;T)|^2$ was analyzed elsewhere [9], here the analysis is restricted to a comparison of $|\tilde{\rho}(R,\omega;T)|^2$ with its counterpart $|\tilde{j}(R,\omega;T)|^2$. In general, both power spectra display well the Bohr frequencies $\omega_{m,n=m+1}$.

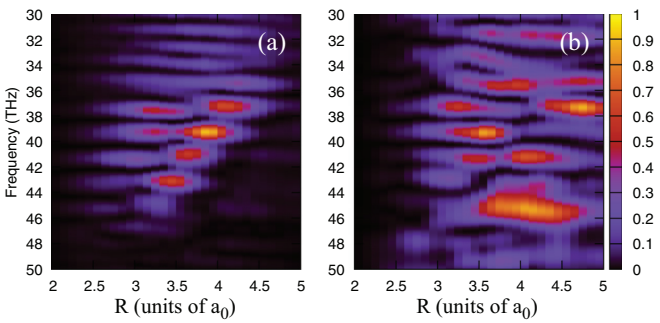

FIG. 3. (Color online) Power spectra of a D_2^+ molecular ion: (a) power spectrum of the constructed nuclear probability density $[|\tilde{\rho}(R,\omega;T=800\,\text{fs})|^2]$ from experimental data, (b) power spectrum of the deduced nuclear flux density $[|\tilde{j}(R,\omega;T=800\,\text{fs})|^2]$.

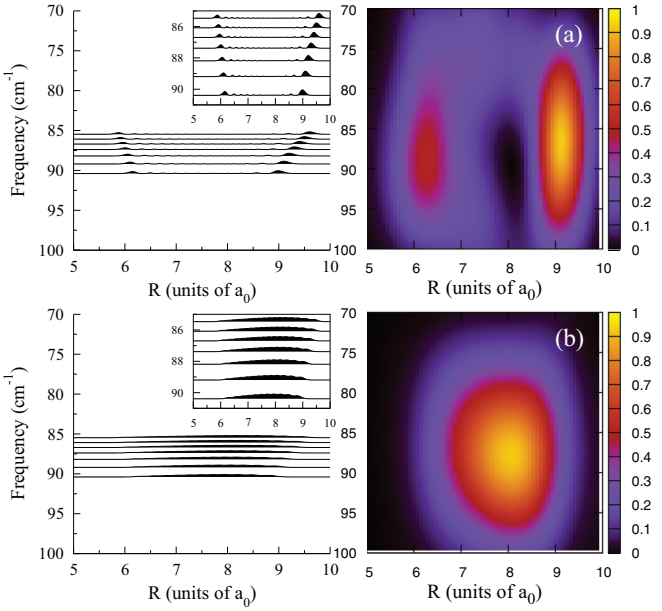

FIG. 4. (Color online) Power spectra of a Na_2 molecule vibrating in the $2^1\Pi_g$ electronic state: (a) power spectrum of the constructed nuclear probability density $[|\tilde{\rho}(R,\omega;T=1800\,\text{fs})|^2]$ from experimental data, (b) power spectrum of the deduced nuclear flux density $[|\tilde{j}(R,\omega;T=1800\,\text{fs})|^2]$. On the left $|\chi_m(R)\chi_n(R)|^2$ (upper panel) and $|\chi_m(R)d\chi_n(R)/dR - \chi_n(R)d\chi_m(R)/dR|^2$ (lower panel).

However, the spatial behavior of $|\tilde{j}(R,\omega;T)|^2$ is quite unexpected. It is a consequence of the mixing of the $^2\Sigma_g{}^+(1s\sigma_g)$ state and the $^2\Sigma_u{}^+(2p\sigma_u)$ state mediated by the laser field [9]. This observation is supported by the quantum effect (QE3) described in Ref. [3], which allows round trips of the nuclear flux density $j(R,t)$ to large internuclear distances, while the nuclear probability density stays localized at intermediate internuclear distances.

Finally, we examine the $Na_2(^2\Pi_g)$ system. Figures 4(a) and 4(b) display, respectively, the power spectrum for the constructed probability density [1] and that for the deduced flux density [3] of a Na_2 molecule vibrating in the $2^1\Pi_g$ electronic state. Unfortunately, because of the relatively short time delay (ca. 2 ps) of the pump-probe experiment, the individual frequencies are not resolved. Nevertheless, we can discuss the gross features of the power spectra. Notice that the power spectrum of the probability density is localized around two internuclear distances, at $R \sim 6a_0$ and at $R \sim 9a_0$, while the spectrum of the flux density is distributed along the internuclear distance. Three photons are involved in the pump-probe experiment with the Na_2 molecule. The first two photons create the wave packet in the $2^1\Pi_g$ electronic state via $A^1\Sigma_u{}^+$ intermediate state, i.e., $X^1\Sigma_g{}^+ \rightarrow A^1\Sigma_u{}^+ \rightarrow 2^1\Pi_g$. The third photon then ionizes the $2^1\Pi_g$ state. Investigation [14] of the dynamical aspects of this multiphoton process show that the transition $A^1\Sigma_u{}^+ \rightarrow 2^1\Pi_g$ occurs only at the inner turning point. This implies that a limited number of vibrational eigenstates contribute to the $2^1\Pi_g$ wave packet. Thus, absorption of two photons induces transitions from $X^1\Sigma_g{}^+, n' = 0$ to the vibrational levels $n = 11$–18 of the $2^1\Pi_g$ state. The left panels of Fig. 4 show $|\chi_m(R)\chi_n(R)|^2$

and $|\chi_m(R)d\chi_n(R)/dR - \chi_n(R)d\chi_m(R)/dR|^2$ for the relevant vibrational eigenstates, i.e., $n = 11$–18. The potential energy curve of the $2^1\Pi_g$ state reported in Ref. [15] was employed for the calculation of the nuclear eigenstates $\chi_n(R)$. Thus, the main trend of the group of frequencies $\omega_{m,n=m+1}$ expected from the product of the eigenstates $\chi_m(R)$ and $\chi_{m+1}(R)$ compares well with the experimental results. In other words, the power spectrum of the density is distributed around the inner and the outer turning points of the potential well [as are all the $|\chi_m(R)\chi_n(R)|^2$], while spectrum of the flux density is distributed along the internuclear distance [as are all the $|\chi_m(R)d\chi_n(R)/dR - \chi_n(R)d\chi_m(R)/dR|^2$].

IV. SUMMARY

This paper demonstrates that Fourier analysis of the nuclear flux density is a valuable tool for the construction of the potential energy curves as well as for the depiction of the inflection points of the vibrational eigenstates $\chi_n(R)$. It is shown that this new observable supplements its counterpart the nuclear probability density, in both the space-time and the space-frequency domains. The ideas developed here were first suggested by quantum-dynamical calculations in the $D_2{}^+(^2\Sigma_g{}^+)$ molecular ion, and then applied to the $D_2{}^+$ molecular ion and the Na_2 molecule, for which the required experimental data are available [1,2]. Finally we point out that the diagonal terms $|\chi_n(R)|^2$ (probability density distribution of the eigenstates) in Eq. (4) do not appear in the Fourier analysis because they become time independent, playing the role of constant background in the time evolution of $\rho(R,t)$. They consistently vanish in the flux density $j(R,t)$ with no possibility of appearing in Eq. (5). However, such an image of the eigenstates has been constructed experimentally for the $H_2{}^+$ molecular ion by means of a technique combining dissociation via electron attachment with cold-target-recoil-ion-momentum spectroscopy [16]. So far, one can experimentally obtain $|\chi_n(R)|^2$ (see Ref. [16]), $|\chi_m(R)\chi_n(R)|^2$ (see Ref. [9]), and $|\chi_m(R)d\chi_n(R)/dR - \chi_n(R)d\chi_m(R)/dR|^2$, as shown here.

ACKNOWLEDGMENTS

The author would like to express his gratitude to T. Baumert (Kassel), Professor J. Ullrich (Heidelberg and Braunschweig), and Dr. R. Moshammer (Heidelberg) for providing the experimental data for the nuclear densities of the vibrating $Na_2(^1\Pi_g)$ and $D_2{}^+(^2\Sigma_g{}^+)$ as published in Refs. [1,2]. He is also grateful to Professor D. J. Diestler (Lincoln), Professor J. Manz (Berlin), and Professor B. Paulus (Berlin) for the continuous support. Computing Services Unit of the Zentraleinrichtung für Datenverarbeitung (ZEDAT) at Freie Universität Berlin is gratefully acknowledged for allocation of computer time. This work was supported by Deutsche Forschungsgemeinschaft under Grant No. PE 2297/1-1.

[1] T. Frohnmeyer and T. Baumert, Appl. Phys. B **71**, 259 (2000).
[2] T. Ergler, A. Rudenko, B. Feuerstein, K. Zrost, C. D. Schröter, R. Moshammer, and J. Ullrich, Phys. Rev. Lett. **97**, 193001 (2006).
[3] J. Manz, J. F. Pérez-Torres, and Y. Yang, Phys. Rev. Lett. **111**, 153004 (2013).
[4] B. Feuerstein and U. Thumm, Phys. Rev. A **67**, 063408 (2003).
[5] J. H. Eberly, N. B. Narozhny, and J. J. Sanchez-Mondragon, Phys. Rev. Lett. **44**, 1323 (1980).
[6] I. S. Averbukh, M. J. J. Vrakking, D. M. Villeneuve, and A. Stolow, Phys. Rev. Lett. **77**, 3518 (1996).
[7] A. Rudenko, T. Ergler, B. Feuerstein, K. Zrost, C. Schröter, R. Moshammer, and J. Ullrich, Chem. Phys. **329**, 193 (2006).
[8] E. Schrödinger, Quantizierung als Eigenwertproblem (Vierte Mitteilung), Ann. Phys. (Leipzig) **81**, 109 (1926).
[9] B. Feuerstein, T. Ergler, A. Rudenko, K. Zrost, C. D. Schröter, R. Moshammer, J. Ullrich, T. Niederhausen, and U. Thumm, Phys. Rev. Lett. **99**, 153002 (2007).
[10] M. Magrakvelidze, A. Kramer, K. Bartschat, and U. Thumm, J. Phys. B: At. Mol. Opt. Phys. **47**, 124003 (2014).
[11] U. Thumm, T. Niederhausen, and B. Feuerstein, Phys. Rev. A **77**, 063401 (2008).
[12] J. Manz, J. F. Pérez-Torres, and Y. Yang, J. Phys. Chem. A **118**, 8411 (2014).
[13] A. D. Bandrauk, E. Aubanel, and S. Chelkowski, in *Femtosecond Chemistry*, edited by J. Manz and L. Wöste (VCH Verlagsgesellschaft, Weinheim, 1995), p. 731.
[14] T. Baumert, B. Bühler, M. Grosser, R. Thalweiser, V. Weiss, and E. Wiedenmann, J. Phys. Chem. **95**, 8103 (1991).
[15] G.-H. Jeung, Phys. Rev. A **35**, 26 (1987).
[16] L. P. H. Schmidt, T. Jahnke, A. Czasch, M. Schöffler, H. Schmidt-Böcking, and R. Dörner, Phys. Rev. Lett. **108**, 073202 (2012).